European Journal of Mechanics A/Solids 39 (2013) 291–297

Contents lists available at SciVerse ScienceDirect

European Journal of Mechanics A/Solids

journal homepage: www.elsevier.com/locate/ejmsol

Strength of graphene in biaxial tension

K. Tuleubekov [a], K.Y. Volokh [b,c,*], H. Stolarski [a], S.G. Mogilevskaya [a]

[a] Department of Civil Engineering, University of Minnesota, Minneapolis, USA
[b] Department of Structural Engineering, Ben-Gurion University of the Negev, Beer Sheva, Israel
[c] Faculty of Civil and Environmental Engineering, Technion – Israel Institute of Technology, Haifa, Israel

ARTICLE INFO

Article history:
Received 9 September 2012
Accepted 19 December 2012
Available online 5 January 2013

Keywords:
Graphene
Strength
Failure
Tersoff–Brenner potential
Atomic relaxation
Crystal

ABSTRACT

A simple analytical study of a single-atom-thick sheet of graphene under biaxial tension is presented. It is based on the combination of the approaches of continuum and molecular mechanics. On the molecular level the Tersoff-Brenner potential with a modified cut-off function is used as an example. Transition to a continuum description is achieved by employing the Cauchy–Born rule. In this analysis the graphene sheet is considered as a crystal composed of two simple Bravais lattices and the mutual atomic relaxation between these lattices is taken into account. Following this approach a critical failure surface is produced for strains in biaxial tension. The adopted methodology is discussed in the context of the alternative approaches.

1. Introduction

For a long time theoretical skepticism prevailed concerning the possibility to create one-atom-thick graphene sheets. The skepticism was based upon the considerations of instabilities of graphene. Nonetheless, Novoselov et al. (2005) succeeded in isolating a one-atom-thick sheet of graphene. This exciting experimental finding led to the explosion of interest in the studies of graphene sheets in view of their potential applications in physics, material science, and engineering (Geim and Novoselov, 2007).

In recent years a number of analytical studies of the mechanical properties of graphene have been reported, e.g. Khare et al. (2007), Liu et al. (2007), Reddy et al. (2006), Zhou and Huang (2008), Lu and Huang (2009), Lee et al. (2008), Wei et al. (2009), Marianetti and Yevick (2010), Zhao and Aluru (2010). Some of them employ very advanced and computationally involved techniques, such as Density Functional Theory and its various versions. The goal of the present paper is to suggest a simple approach to study the same problem and examine its validity.

The analysis presented here is a modification of the earlier approach by Volokh (2012), who obtained the failure surface for graphene under biaxial tension using a similar technique. Volokh (2012) adopted a continuum-atomistic approach wherein the strain energy of a 2D graphene sheet was defined with the help of the Tersoff–Brenner empirical potential (Tersoff, 1988; Brenner, 1990) for individual bonds. The multiscale approach allowed considering the problem analytically without numerical simulations. In that paper no atomic relaxation was included.

In the present study we elaborate on Volokh's (2012) results by accounting for the atomic relaxation. For this purpose, we consider the graphene sheet as a superposition of two simple atomic Bravais lattices which can move with respect to each other during deformation. This requires introduction of an additional degree of freedom – the internal displacement $\boldsymbol{\Delta}$–while still permitting for a simple analytical calculations. In addition, in this paper we introduce a new cut-off function, which is virtually indistinguishable from that of the original Tersoff–Brenner potential and is more convenient in numerical simulations, as it possesses higher degree of smoothness. The model presented in the present work, which includes atomic relaxation, provides means to examine the influence of additional degrees of freedom on the strength of graphene.

2. Governing equations: continuum-atomistic coupling

Coupling of continuum and molecular mechanics can dramatically simplify the analysis of the mechanical behavior of graphene. In the present section the major results of the coupling relevant to the subsequent considerations are reviewed.

We model atomic interactions by using the Tersoff–Brenner environmental potential defined as follows (Tersoff, 1988; Brenner, 1990)

* Corresponding author. Faculty of Civil and Environmental Engineering, Technion – Israel Institute of Technology, Haifa, Israel.
E-mail address: cvolokh@technion.ac.il (K.Y. Volokh).

0997-7538/$ – see front matter © 2012 Elsevier Masson SAS. All rights reserved.
http://dx.doi.org/10.1016/j.euromechsol.2012.12.006

$$U(r_{ij}) = \frac{D}{S-1} f_c(r_{ij}) \left\{ \exp\left[-\sqrt{2S}\beta(r_{ij}-R_{ij}) \right] - \frac{S}{2}(B_{ij} + B_{ji}) \exp\left[-\sqrt{2/S}\beta(r_{ij}-R_{ij}) \right] \right\}, \quad (1)$$

$$f_c(r_{ij}) = H(r_{ij}) - H(r_{ij}-a_1) + \frac{1}{2}\left\{ 1 + \cos\frac{\pi(r_{ij}-a_1)}{a_2-a_1} \right\} \times \{ H(r_{ij}-a_1) - H(r_{ij}-a_2) \}, \quad (2)$$

$$B_{ij} = \left\{ 1 + \sum_{k(\neq i,j)} a_0 \left(1 + \frac{c_0^2}{d_0^2} - \frac{c_0^2}{d_0^2 + \left(1+\cos\varphi_{ijk}\right)^2} \right) f_c(r_{ik}) \right\}^{-\delta}, \quad (3)$$

$$R_{ij} = \sqrt{\mathbf{R}_{ij}\cdot\mathbf{R}_{ij}}, \quad \mathbf{R}_{ij} = \mathbf{R}_j - \mathbf{R}_i, \quad (4)$$

$$r_{ij} = \sqrt{\mathbf{r}_{ij}\cdot\mathbf{r}_{ij}}, \quad \mathbf{r}_{ij} = \mathbf{r}_j - \mathbf{r}_i, \quad (5)$$

$$\cos\varphi_{ijk} = \frac{\mathbf{r}_{ij}\cdot\mathbf{r}_{ik}}{r_{ij}r_{ik}}, \quad (6)$$

where $\mathbf{R}_i$ and $\mathbf{r}_i$ are the referential and current positions of the ith atom and the Heaviside unit step function has been used

$$H(z) = \begin{cases} 1, & z \geq 0 \\ 0, & z < 0 \end{cases}.$$

In the case of graphene the constants can be defined as follows: $a_0 = 0.00020813$; $c_0 = 330$; $d_0 = 3.5$; $\delta = 0.5$; $D = 6.0$ eV; $S = 1.22$; $\beta = 21$ nm^{-1}; $a_1 = 0.17$ nm; $a_2 = 0.20$ nm; and $R_{ij} = R = 0.142$ nm is the equilibrium bond length.

The cut-off function of Eq. (2) includes the Heaviside step function that is rather inconvenient to use in computations. For that reason we introduce a new cut-off function defined as follows

$$f_c(r) = \frac{1}{2}\left(1 - \mathrm{erf}\left(\frac{r-(a_1+a_2)/2}{0.0095} \right) \right), \quad (7)$$

where

$$\mathrm{erf}(r) = \frac{2}{\sqrt{\pi}} \int_0^r \exp\left(-t^2\right) \mathrm{d}t \quad (8)$$

The original and the new cut-off functions are plotted in Fig. 1 and, as can be seen there, they are virtually indistinguishable.

In addition, using the new cut-off function of Eq. (7), we solved the problem considered by Volokh (2012) and found that the results obtained with the original and the new cut-off functions are practically identical. Thus, in the subsequent analysis we will use the cut-off function of Eq. (7).

Generally, the potentials of Eq. (1) should be defined and summed overall atoms comprising the graphene sheet. However, we will restrict our considerations to the homogeneous deformations, which naturally suggest the use of the methods of continuum mechanics. In continuum mechanics the atomistic or molecular structure of material is approximated by a continuously distributed set of the so-called material points. The continuum material point is an abstraction that is used to designate a small representative volume of real material including many atoms and molecules. A material point that occupies position $\mathbf{x}$ in the reference or initial configuration of continuum moves to position $\mathbf{y}(\mathbf{x})$ in the current configuration of continuum. The *homogeneous deformation* in the vicinity of the material point can be described by the deformation gradient tensor

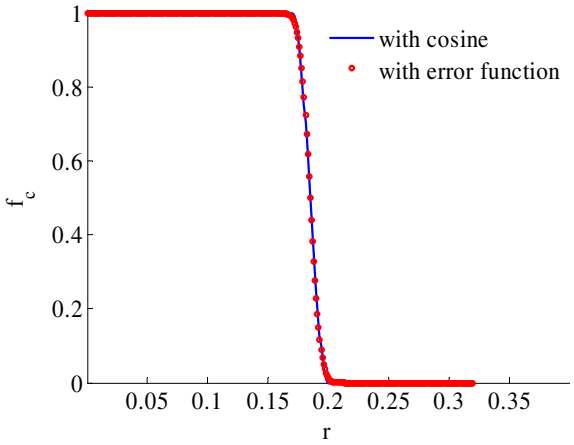

Fig. 1. Cut-off function.

$$\mathbf{F} = \frac{\partial \mathbf{y}}{\partial \mathbf{x}}. \quad (9)$$

With the help of this tensor we can relate the relative atomic positions before and after deformation as follows

$$\mathbf{r}_{ij} = \mathbf{F}\mathbf{R}_{ij}. \quad (10)$$

Eq. (10) links atomistic and continuum descriptions. This link is tacitly assumed in the classical continuum mechanics where the infinitesimal representative material volumes deform locally in the homogeneous manner. In crystal elasticity (Beatty and Hayes, 2005), the multiscale link of Eq. (10) is often referred to as the Cauchy–Born rule (Born and Huang, 1954; Weiner, 1983; Tadmor et al., 1996). Using Eq. (10) we can write the density of the stored energy in the form

$$\psi(\mathbf{C}) = \frac{1}{2V_0} \sum_{i,j} U(r_{ij}(\mathbf{C})), \quad (11)$$

$$r_{ij} = \left|\mathbf{F}\mathbf{R}_{ij}\right| = \sqrt{\mathbf{R}_{ij}\cdot\mathbf{C}\mathbf{R}_{ij}}, \quad \mathbf{C} = \mathbf{F}^T\mathbf{F}, \quad (12)$$

where V_0 is the initial volume occupied by the atomic assembly and $\mathbf{C}$ is the so-called right Cauchy–Green tensor.

By introducing Eqs. (11) and (12) we established transition to a continuum description of the atomic assembly. After defining the stored energy by Eq. (11) we can define the total energy of the assembly in the form

$$\Pi(\mathbf{y}) = \int \psi \mathrm{d}V_0 - \int \bar{\mathbf{t}}_0 \cdot \mathbf{y} \mathrm{d}S_0, \quad (13)$$

where $\bar{\mathbf{t}}_0$ is a prescribed surface traction.

For the sake of simplicity we assume that surface tractions are 'dead', that is independent of surface placements, and the inertia and body forces are absent.

Equating the first variation of the total energy, with respect to the position in the current configuration of the graphene, to zero

$$\delta\Pi(\mathbf{y}) = 0 \quad (14)$$

the equilibrium equations and natural boundary conditions on tractions are obtained by virtue of arbitrary $\delta\mathbf{y}$

$$\mathrm{Div}\mathbf{P} = \mathbf{0} \quad \text{on } \Omega_0, \quad \mathbf{P}\mathbf{n}_0 = \bar{\mathbf{t}}_0 \quad \text{on } \partial\Omega_0, \quad (15)$$

where 'Div' is computed with respect to the referential coordinates $\mathbf{x}$; Ω_0 and $\partial\Omega_0$ designate the initial configuration of the assembly and its bounding surface respectively; $\mathbf{n}_0$ is the unit outward normal to the surface in the initial configuration; and $\mathbf{P}$ is the so-called 1st Piola–Kirchhoff stress tensor defined by the hyperelastic constitutive law

$$\mathbf{P} = 2\mathbf{F}\frac{\partial\psi}{\partial\mathbf{C}}. \tag{16}$$

It should be noted that only those solutions of Eq. (15) are stable and observable which obey the condition of the positive definiteness of the second variation of the total energy (for every variation $\delta\mathbf{y}$)

$$\delta^2\Pi(\mathbf{y}) > 0. \tag{17}$$

We notice also that in the case of homogeneous deformations considered in the present work the 1st PK stress is constant and, consequently, the equilibrium condition of Eq. $(15)_1$ is satisfied automatically. The constant stresses can be found from the traction condition of Eq. $(15)_2$ or, in the case of the displacement control, the stresses are calculated from the constitutive equation, Eq. (16).

In the case of the homogeneous deformation, the approach of continuum mechanics described by Eqs. (13)–(17) is applicable to atomic assemblies forming a single simple Bravais lattice. However, a graphene sheet is composed of two simple Bravais lattices – Fig. 2.

Two simple lattices comprising graphene can move with respect to each other independently. Thus, an additional vector of the lattice shift should be introduced in Eq. (10) for one of the two Bravais lattices (yellow, in the subsequent analysis) as follows

$$\mathbf{r}_{ij} = \mathbf{F}\mathbf{R}_{ij} + \boldsymbol{\gamma} = \mathbf{F}(\mathbf{R}_{ij} + \boldsymbol{\Delta}), \tag{18}$$

where vectors $\boldsymbol{\gamma}$ and $\boldsymbol{\Delta} = \mathbf{F}^{-1}\boldsymbol{\gamma}$ describe a possible shift between the two lattices. These vectors are introduced to increase the number of possible equilibrium states and allow for the relaxation of the atomic positions of the lattices, if any.

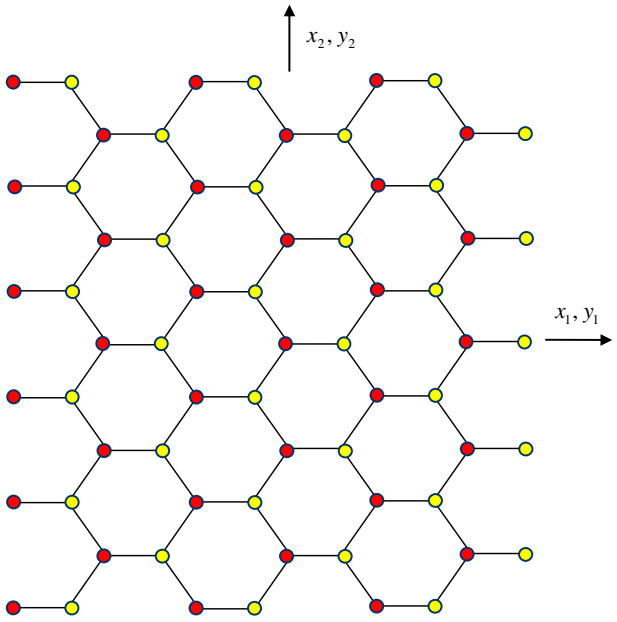

Fig. 2. Graphene sheet composed of two (red and yellow) simple Bravais lattices. (For interpretation of the references to color in this figure legend, the reader is referred to the web version of this article.)

The shift vector is determined by minimizing the stored energy density with respect to $\boldsymbol{\Delta}$ (Weiner, 1983; Tadmor et al., 1999; Arroyo and Belytschko, 2002, 2004; Huang et al., 2006; Zhang et al., 2004; Zhou and Huang, 2008; Wu et al., 2008)

$$\frac{\partial\psi(\mathbf{C},\boldsymbol{\Delta})}{\partial\boldsymbol{\Delta}} = 0. \tag{19}$$

3. Specialization

In this section we specialize the formulae considered in the previous section for the case of biaxial tension of a graphene sheet. Since the sheet is made of a single atomic layer and out-of-plane strains and stresses might be difficult to interpret, we restrict considerations to the in-plane 2D continuum mechanics.

We define the Cartesian axes in the plane of the sheet as shown in Fig. 2. Thus, the two-dimensional deformation can be described as follows

$$y_1 = \lambda_1 x_1, \quad y_2 = \lambda_2 x_2, \tag{20}$$

$$\mathbf{F} = \lambda_1\mathbf{e}_1\otimes\mathbf{e}_1 + \lambda_2\mathbf{e}_2\otimes\mathbf{e}_2, \quad \mathbf{C} = \lambda_1^2\mathbf{e}_1\otimes\mathbf{e}_1 + \lambda_2^2\mathbf{e}_2\otimes\mathbf{e}_2, \tag{21}$$

where $\mathbf{e}_1$ and $\mathbf{e}_2$ are the Cartesian base vectors.

We notice that the initial configuration of the graphene sheet, shown in Fig. 2, has vertical and horizontal axes of symmetry. At the same time the biaxial tensile loads we consider should preserve these symmetries in the deformed configuration up to the critical point of the sheet instability. This reasoning excludes vertical shifts between the simple Bravais lattices comprising the sheet; otherwise, the symmetries would be destroyed. However, the horizontal shift between the lattices preserves these symmetries and it is admissible – Fig. 3 – Consequently we have

$$\boldsymbol{\Delta} = \Delta\mathbf{e}_1. \tag{22}$$

Substituting Eqs. (21) and (22) in Eq. (18) we obtain

$$\mathbf{r}_{ij} = \mathbf{F}\mathbf{R}_{ij} + \lambda_1\Delta\mathbf{e}_1. \tag{23}$$

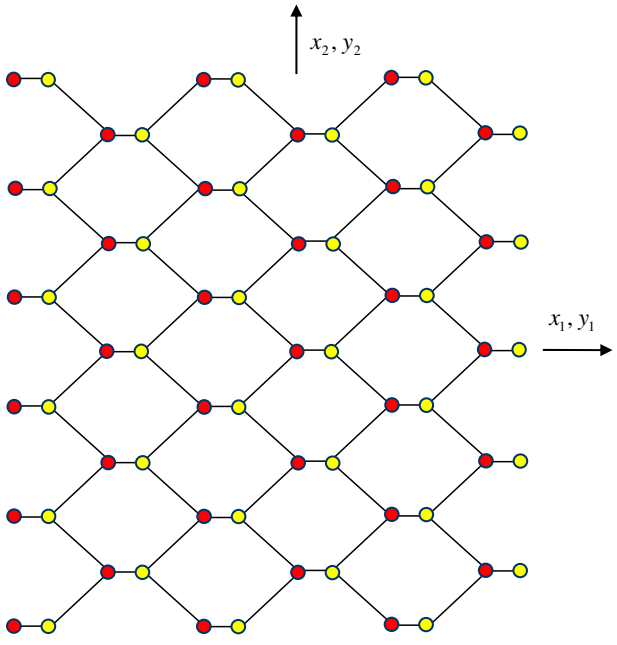

Fig. 3. Graphene sheet with a horizontal mutual shift of two simple Bravais lattices.

It is possible to restrict further analysis to the graphene pattern shadowed in Fig. 4.

In this case the stored energy function defined per area rather than per volume can be written as follows

$$A_0\psi = U(r_{12}) + U(r_{13}) + U(r_{14}), \tag{24}$$

where $A_0 = 3\sqrt{3}R^2/2$ is the area of the shadowed pattern in the reference configuration.

We determine the first term on the right hand side of Eq. (24) as follows

$$U(r_{12}) = \frac{D}{S-1} f_c(r_{12}) \Big\{ \exp\Big[-\sqrt{2S}\beta(r_{12}-R)\Big] - \frac{S}{2}(B_{12}+B_{21})\exp\Big[-\sqrt{2/S}\beta(r_{12}-R)\Big]\Big\}, \tag{25}$$

where

$$\begin{cases} B_{12} = \left\{ 1 + \sum\limits_{k=3,4} a_0 \left(1 + \dfrac{c_0^2}{d_0^2} - \dfrac{c_0^2}{d_0^2 + (1+\cos\varphi_{12k})^2} \right) f_c(r_{1k}) \right\}^{-\delta} \\ B_{21} = \left\{ 1 + \sum\limits_{k=5,6} a_0 \left(1 + \dfrac{c_0^2}{d_0^2} - \dfrac{c_0^2}{d_0^2 + (1+\cos\varphi_{21k})^2} \right) f_c(r_{2k}) \right\}^{-\delta}. \end{cases} \tag{26}$$

To calculate the potentials of Eqs. (25)–(26) we define the reference relative atomic positions as follows

$$\begin{cases} \mathbf{R}_{12} = R\mathbf{e}_1 \\ \mathbf{R}_{13} = -\dfrac{R}{2}\left(\mathbf{e}_1 + \sqrt{3}\mathbf{e}_2\right) \\ \mathbf{R}_{14} = -\dfrac{R}{2}\left(\mathbf{e}_1 - \sqrt{3}\mathbf{e}_2\right). \\ \mathbf{R}_{21} = -\mathbf{R}_{12} \\ \mathbf{R}_{25} = -\mathbf{R}_{13} \\ \mathbf{R}_{26} = -\mathbf{R}_{14} \end{cases} \tag{27}$$

Substituting expressions of Eq. (27) into that of Eq. (23) we get the current relative atomic positions

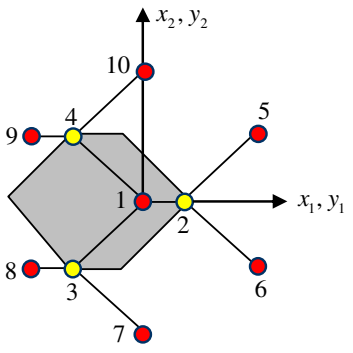

Fig. 4. Graphene pattern is shadowed in gray.

$$\begin{cases} \mathbf{r}_{12} = \lambda_1(R+\Delta)\mathbf{e}_1 \\ \mathbf{r}_{13} = \left(\Delta - \dfrac{R}{2}\right)\lambda_1\mathbf{e}_1 - \dfrac{R\sqrt{3}}{2}\lambda_2\mathbf{e}_2 \\ \mathbf{r}_{14} = \left(\Delta - \dfrac{R}{2}\right)\lambda_1\mathbf{e}_1 + \dfrac{R\sqrt{3}}{2}\lambda_2\mathbf{e}_2. \\ \mathbf{r}_{21} = -\mathbf{r}_{12} \\ \mathbf{r}_{25} = -\mathbf{r}_{13} \\ \mathbf{r}_{26} = -\mathbf{r}_{14} \end{cases} \tag{28}$$

Furthermore, substituting expressions of Eq. (28) into those of Eqs. (5) and (6) we have

$$r_{12} = \lambda_1(R+\Delta), \quad r_{13} = r_{14} = r_{25} = r_{26} = \sqrt{\left(\Delta - \frac{R}{2}\right)^2\lambda_1^2 + \frac{3}{4}\lambda_2^2R^2}, \tag{29}$$

$$\cos\varphi_{123} = \cos\varphi_{124} = \cos\varphi_{215} = \cos\varphi_{216} = \frac{\left(\Delta - \frac{R}{2}\right)\lambda_1}{\sqrt{\left(\Delta - \frac{R}{2}\right)^2\lambda_1^2 + \frac{3}{4}\lambda_2^2R^2}}. \tag{30}$$

Expressions of Eqs. (29) and (30) combined with those of Eq. (26) yield

$$B_{12} = B_{21}. \tag{31}$$

The second term on the right hand side of Eq. (24), calculated in a similar fashion, yields

$$U(r_{13}) = \frac{D}{S-1} f_c(r_{13}) \Big\{ \exp\Big[-\sqrt{2S}\beta(r_{13}-R)\Big] - \frac{S}{2}(B_{13}+B_{31})\exp\Big[-\sqrt{2/S}\beta(r_{13}-R)\Big]\Big\}, \tag{32}$$

where

$$\begin{cases} B_{13} = \left\{ 1 + \sum\limits_{k=2,4} a_0 \left(1 + \dfrac{c_0^2}{d_0^2} - \dfrac{c_0^2}{d_0^2 + (1+\cos\varphi_{13k})^2} \right) f_c(r_{1k}) \right\}^{-\delta} \\ B_{31} = \left\{ 1 + \sum\limits_{k=7,8} a_0 \left(1 + \dfrac{c_0^2}{d_0^2} - \dfrac{c_0^2}{d_0^2 + (1+\cos\varphi_{31k})^2} \right) f_c(r_{3k}) \right\}^{-\delta}. \end{cases} \tag{33}$$

To evaluate expressions of Eqs. (32)–(33) we use Eq. $(28)_{1-3}$ using the following reference relative atomic positions

$$\begin{cases} \mathbf{R}_{31} = -\mathbf{R}_{13} \\ \mathbf{R}_{37} = -\mathbf{R}_{14}. \\ \mathbf{R}_{38} = -\mathbf{R}_{12} \end{cases} \tag{34}$$

Substituting Eq. (34) in Eq. (23) we get

$$\begin{cases} \mathbf{r}_{31} = -\mathbf{r}_{13} \\ \mathbf{r}_{37} = -\mathbf{r}_{14}. \\ \mathbf{r}_{38} = -\mathbf{r}_{12} \end{cases} \tag{35}$$

Eq. $(28)_{1-3}$ and (35) together with Eqs. (5) and (6) render the following results

$$r_{12} = r_{38} = \lambda_1(R+\Delta), \quad r_{13} = r_{14} = r_{37} = \sqrt{\left(\Delta - \frac{R}{2}\right)^2 \lambda_1^2 + \frac{3}{4}\lambda_2^2 R^2}, \tag{36}$$

$$\cos\varphi_{132} = \cos\varphi_{318} = \frac{\left(\Delta - \frac{R}{2}\right)\lambda_1}{\sqrt{\left(\Delta - \frac{R}{2}\right)^2 \lambda_1^2 + \frac{3}{4}\lambda_2^2 R^2}}, \quad \cos\varphi_{134} = \cos\varphi_{317} = \frac{\left(\Delta - \frac{R}{2}\right)^2 \lambda_1^2 - \frac{3}{4}\lambda_2^2 R^2}{\left(\Delta - \frac{R}{2}\right)^2 \lambda_1^2 + \frac{3}{4}\lambda_2^2 R^2}. \tag{37}$$

Substituting Eqs. (36) and (37) in Eqs. (32) and (33) we conclude that

$$B_{13} = B_{31}. \tag{38}$$

Finally, we specify the third term on the right hand side of Eq. (24)

$$U(r_{14}) = \frac{D}{S-1} f_c(r_{14}) \left\{ \exp\left[-\sqrt{2S}\beta(r_{14} - R)\right] - \frac{S}{2}(B_{14} + B_{41}) \exp\left[-\sqrt{2/S}\beta(r_{14} - R)\right] \right\}, \tag{39}$$

where

$$\begin{cases} B_{14} = \left\{ 1 + \sum\limits_{k=2,3} a_0 \left(1 + \frac{c_0^2}{d_0^2} - \frac{c_0^2}{d_0^2 + (1+\cos\varphi_{14k})^2} \right) f_c(r_{1k}) \right\}^{-\delta} \\ B_{41} = \left\{ 1 + \sum\limits_{k=9,10} a_0 \left(1 + \frac{c_0^2}{d_0^2} - \frac{c_0^2}{d_0^2 + (1+\cos\varphi_{41k})^2} \right) f_c(r_{4k}) \right\}^{-\delta} \end{cases}. \tag{40}$$

To evaluate expressions involved in Eqs. (39) and (40) we use Eq. $(28)_{1-3}$ with the following reference relative atomic positions:

$$\begin{cases} \mathbf{R}_{41} = -\mathbf{R}_{14} \\ \mathbf{R}_{410} = -\mathbf{R}_{13} \\ \mathbf{R}_{49} = -\mathbf{R}_{12} \end{cases}. \tag{41}$$

Substituting expressions of Eq. (41) in Eq. (23) we get

$$\begin{cases} \mathbf{r}_{41} = -\mathbf{r}_{14} \\ \mathbf{r}_{410} = -\mathbf{r}_{13} \\ \mathbf{r}_{49} = -\mathbf{r}_{12} \end{cases}. \tag{42}$$

Using expressions of Eq. $(28)_{1-3}$, (42) in Eqs. (5) and (6) we obtain

$$r_{12} = r_{49} = \lambda_1(R+\Delta), \quad r_{13} = r_{14} = r_{410} = \sqrt{\left(\Delta - \frac{R}{2}\right)^2 \lambda_1^2 + \frac{3}{4}\lambda_2^2 R^2}, \tag{43}$$

$$\cos\varphi_{142} = \cos\varphi_{419} = \frac{\left(\Delta - \frac{R}{2}\right)\lambda_1}{\sqrt{\left(\Delta - \frac{R}{2}\right)^2 \lambda_1^2 + \frac{3}{4}\lambda_2^2 R^2}}, \quad \cos\varphi_{143} = \cos\varphi_{4110} = \frac{\left(\Delta - \frac{R}{2}\right)^2 \lambda_1^2 - \frac{3}{4}\lambda_2^2 R^2}{\left(\Delta - \frac{R}{2}\right)^2 \lambda_1^2 + \frac{3}{4}\lambda_2^2 R^2}. \tag{44}$$

Substituting Eqs. (43) and (44) in Eqs. (39) and (40) we observe

$$B_{14} = B_{41}. \tag{45}$$

Thus, the stored energy of Eq. (24) is completely defined.

4. Results

In the previous sections the stored energy ψ was completely defined as a function of stretches λ_1, λ_2 and the lattice relaxation shift Δ. The latter shift can be calculated as a function of stretches from the condition of Eq. (19)

$$\frac{\partial \psi(\lambda_1, \lambda_2, \Delta)}{\partial \Delta} = 0. \tag{46}$$

The deformation of the graphene sheet is stable as long as the second variation of the total energy is positive

$$\delta^2 \Pi(\lambda_1, \lambda_2, \Delta) = A_0^2 \delta^2 \psi(\lambda_1, \lambda_2, \Delta) > 0 \tag{47}$$

It is emphasized that in the above development the deformation is homogeneous and the surface tractions are 'dead'. In addition, the relations of Eq. (20) specifying the deformed configuration of graphene in terms of stretches has been used in Eq. (47).

For the second variation of Eq. (47) to be positive, the following Hessian matrix

$$\mathbf{M} = \begin{bmatrix} \frac{\partial^2 \psi}{\partial \lambda_1^2} & \frac{\partial^2 \psi}{\partial \lambda_1 \partial \lambda_2} & \frac{\partial^2 \psi}{\partial \lambda_1 \partial \Delta} \\ \frac{\partial^2 \psi}{\partial \lambda_1 \partial \lambda_2} & \frac{\partial^2 \psi}{\partial \lambda_2^2} & \frac{\partial^2 \psi}{\partial \lambda_2 \partial \Delta} \\ \frac{\partial^2 \psi}{\partial \lambda_1 \partial \Delta} & \frac{\partial^2 \psi}{\partial \lambda_2 \partial \Delta} & \frac{\partial^2 \psi}{\partial \Delta^2} \end{bmatrix} \tag{48}$$

evaluated at the equilibrium point (the parameter of the relaxation shift, Δ, is computed from Eq. (46)) must be positive definite. This implies that all principal minors of matrix **M** must be positive and stability of graphene sheet is lost when any one of them becomes negative.

One way of trying to determine the boundary between the stable and unstable regions is based on the observation that for $\lambda_1 = \lambda_2$ (isotropic expansion of lattice) equilibrium conditions are satisfied with $\Delta = 0$. Thus, any values of $\lambda_1 = \lambda_2$ and $\Delta = 0$ constitute good starting point to determine subsequent values of Δ for incrementally changing λ_1 while keeping λ_2 = constant (or vice-versa). To compute the value of Δ Eq. (46) is solved in an iterative manner. At each step of such analysis all three minors of Hessian matrix **M** are computed and the process continues until one of them becomes negative. The corresponding values of λ_1, λ_2 determine the boundary of the stability region, and the resulting Δ is the lattice shift associated with that point of the boundary.

The loss of stability marks the onset of the material bond rupture with the subsequent failure localization and propagation.

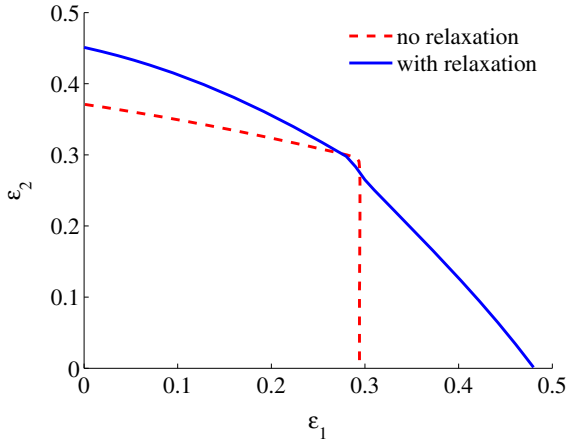

Fig. 5. Critical failure strains in biaxial tension.

Below we will only consider the critical point of the onset of failure without analyzing its localization and propagation.

It is convenient to define the critical failure surface in terms of the engineering strains

$$\varepsilon_1 = \lambda_1 - 1, \quad \varepsilon_2 = \lambda_2 - 1. \tag{49}$$

This failure surface is presented by the solid line in Fig. 5. Dashed line represents the failure surface without relaxation parameter Δ (Volokh, 2012).

It could be seen that the curve obtained with the inclusion of relaxation parameter is significantly different from the one obtained without that parameter. To appreciate the influence the lattice shift Δ has on the overall stable deformation, Fig. 6 provides its value normalized with respect to undeformed lattice dimension R at each point of the stability boundary parameterized by ε_1. A couple of characteristic features can be seen in Fig. 6: (i) extreme values of Δ correspond to uniaxial stretching in either horizontal or vertical direction, (ii) the signs of Δ corresponding to those two directions of stretching are different, as expected.

There is a visible lack of smoothness around the point of the stability boundary corresponding roughly to $\lambda_1 = \lambda_2$, which can be explained by the sensitivity of the numerical analysis used. In this regard we note that to obtain the part of the curve of Fig. 6 located to the left of that point λ_1 had to be kept constant while changing λ_2. To the right of that point the roles of λ_1 and λ_2 were reversed. In view of the fact that the formulas used in the calculations depend on λ_1 and λ_2 in a very different way, and in view of the assumed limited accuracy of the computations, it is natural to expect the errors reflected in Fig. 6. This is particularly true considering that around that point the value of the relaxation parameter Δ is close to zero.

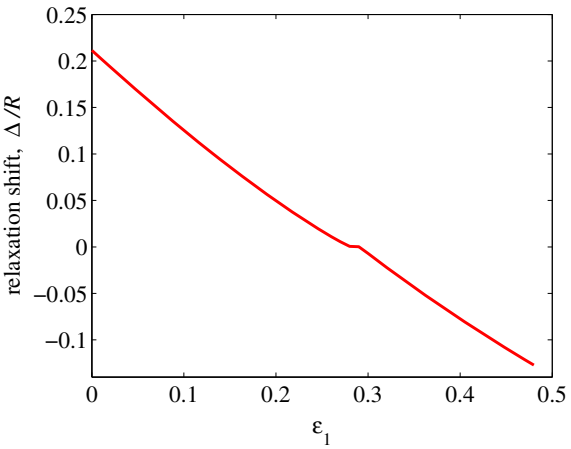

Fig. 6. Relaxation shift versus strain.

5. Conclusions

In this paper we studied a simple analytical procedure to examine strength of graphene in biaxial tension, which is an important aspect of its mechanical behavior. It was accomplished without having to calculate stress–strain relationships. This is in contrast with all previous approaches (e.g. Liu et al., 2007) where the strength could only be deduced from the stress-strain curve. To obtain stress-strain curves the previous authors used (a) various macroscopic stress measures and (b) various definitions of macroscopic stresses through the interatomic forces. Since neither macroscopic stress measures nor their microscopic definitions are unique (Admal and Tadmor, 2010) the limit points on the simulated stress-strain curves cannot be accepted as a unique description of strength. Contrary to the previous works, the global energy analysis performed in the present paper is much more natural and unique.

In our approach the stress-strain curve could also be obtained from Eq. (16) but direct computation of strength is advantageous.

In addition, we introduced a new cut off function in the Tersoff–Brenner potential that is more convenient in numerical analysis of the problem. It was shown that the new cut-off function can be used with virtually no influence on the results of numerical analysis comparing with the original function.

We studied the influence of the relative motion of simple atomic lattices – atomic relaxation – on the results of analysis. It was found that the deformability of graphene at failure was significantly affected by the presence of the atomic relaxation parameter. In purely one dimensional stretching ($\lambda_1 = 1$ or $\lambda_2 = 1$) the inclusion of the relaxation parameter increased the strength of graphene. This is understandable since the additional degree of freedom allows for additional patterns of deformation. For biaxial stretching with equal intensity ($\lambda_1 = \lambda_2$) in both directions, the failure occurs at about the same strains as those without the relaxation parameter. This is also understandable since in this case original hexagonal arrangement of atoms deforms proportionally and no relaxation parameter is needed to maintain equilibrium. Overall, the curve representing strains at failure is significantly smoothened as the result of lattice relaxation. However, as expected, the strains at failure corresponding to two orthogonal direction of stretching are different (strength anisotropy).

Comparing our results to those resulting from the stress-strain curves based on *ab initio* calculations (Liu et al., 2007 and others) the strains at failures we obtained are about twice as big. This could be possibly attributed to two major differences between our approach and the approaches of the other authors. First, as mentioned earlier, there is an ambiguity in the definition of strains and, particularly, stresses. Second, equally significant, is the fact that in the existing approaches the one-dimensional analysis presented there was in fact one-dimensional *stress* analysis ($\sigma_{11} \neq 0$ and $\sigma_{22} = 0$ or vice versa) while in our approach it was one-dimensional *strain* analysis ($\varepsilon_{11} \neq 0$ and $\varepsilon_{22} = 0$ or vice versa). Those are two very different problems more then likely associated with different mechanisms of failure.

In recent publication (Marianetti and Yevick, 2010) it has been found that, when inhomogeneous deformation is allowed, groups of atoms in the grapheme form a new honeycomb arrangement associated with a new failure mechanism. This mechanism corresponds to a significantly smaller failure load than those reported in the literature earlier. Detection of that mechanism was possible by analyzing phonons and observing that there exists an unstable and

rather weak phonon. Detection of such mechanism within our approach would only be possible if the deformation gradient used in our description was allowed to be a function of position. That would mean that a system of partial differential equations would need to be solved, which would significantly complicate the analysis.

Finally, it is important to emphasize that other interatomic potentials can be used within the proposed methodology (e.g. REBO potentials, Brenner et al., 2002) likely leading to somewhat different results. This and other issues alluded to in this Section could be explored in a future work.

References

Admal, N.C., Tadmor, E.B., 2010. A unified interpretation of stress in molecular systems. J. Elast. 100, 63–143.

Arroyo, M., Belytschko, T., 2002. An atomistic-based finite deformation membrane for single layer crystalline films. J. Mech. Phys. Solids 50, 1941–1977.

Arroyo, M., Belytschko, T., 2004. Finite crystal elasticity of carbon nanotubes based on the exponential Cauchy–Born rule. Phys. Rev. B 69, 115415.

Beatty, M.F., Hayes, M.A., 2005. Mechanics and Mathematics of Crystals. Selected Papers of J.L. Ericksen. World Scientific, Singapore.

Born, M., Huang, K., 1954. Dynamical Theory of the Crystal Lattices. Oxford University Press, Oxford.

Brenner, D.W., et al., 2002. A second generation reactive empirical bond order (REBO) potential energy expression for hydrocarbons. J. Phys. Condens. Matter 14, 783–802.

Brenner, D.W., 1990. Empirical potential for hydrocarbons for use in simulating the chemical vapor deposition of diamond films. Phys. Rev. B 42, 9458–9471.

Geim, A.K., Novoselov, K.S., 2007. The rise of graphene. Nat. Mater. 6, 183–191.

Huang, Y., Wu, J., Hwang, K.C., 2006. Thickness of graphene and single-wall carbon nanotubes. Phys. Rev. B 74, 245413.

Khare, R., Mielke, S.L., Paci, J.T., Zhang, S.L., Ballarini, R., Schatz, G.C., Belytschko, T., 2007. Coupled quantum mechanical/molecular mechanical modeling of the fracture of defective carbon nanotubes and graphene sheets. Phys. Rev. B 75, 075412.

Lee, C., Wei, X., Kysar, J.W., Hone, J., 2008. Measurement of the elastic properties and intrinsic strength of monolayer graphene. Science 321, 385–388.

Liu, F., Ming, P.M., Li, J., 2007. Ab initio calculation of ideal strength and phonon instability of graphene under tension. Phys. Rev. B 76, 064120.

Lu, Q., Huang, R., 2009. Nonlinear mechanics of single-atomic-layer graphene sheets. Int. J. Appl. Mech. 3, 443–467.

Marianetti, C.A., Yevick, H.G., 2010. Failure mechanisms of graphene under tension. Phys. Rev. Lett. 105, 245502.

Novoselov, K.S., Jiang, D., Schedin, F., Booth, T.J., Khotkevich, V.V., Morozov, S.V., Geim, A.K., 2005. Two-dimensional atomic crystals. Proc. Natl. Acad. Sci. U. S. A. 102, 10451–10453.

Reddy, C.D., Rajendran, S., Liew, K.M., 2006. Equilibrium configuration and continuum elastic properties of finite sized graphene. Nanotechnology 17, 864–870.

Tadmor, E.B., Ortiz, M., Phillips, R., 1996. Quasicontinuum analysis of defects in solids. Phil. Mag. A 73, 1529–1563.

Tadmor, E.B., Smith, G.S., Bernstein, N., Kaxiras, E., 1999. Mixed finite element and atomistic formulation for complex crystals. Phys. Rev. B 59, 235–245.

Tersoff, J., 1988. New empirical approach for the structure and energy of covalent systems. Phys. Rev. B 37, 6991–7000.

Volokh, K.Y., 2012. On the strength of graphene. J. Appl. Mech. 79, 064501.

Wei, X., Fragneaud, B., Marianetti, C.A., Kysar, J.W., 2009. Nonlinear elastic behavior of graphene: ab initio calculations to continuum description. Phys. Rev. B 80, 205407.

Weiner, J.H., 1983. Statistical Mechanics of Elasticity. Wiley, New York.

Wu, J., Hwang, K.C., Huang, Y., 2008. An atomistic-based finite-deformation shell theory for single-wall carbon nanotubes. J. Mech. Phys. Solids 56, 279–292.

Zhang, P., Jiang, H., Huang, Y., Geubelle, P.H., Hwang, K.C., 2004. An atomistic-based continuum theory for carbon nanotubes: analysis of fracture nucleation. J. Mech. Phys. Solids 52, 977–998.

Zhao, H., Aluru, N.R., 2010. Temperature and strain-rate dependent fracture strength of graphene. J. Appl. Phys. 108, 064321.

Zhou, J., Huang, R., 2008. Internal lattice relaxation of single-layer graphene under in-plane deformation. J. Mech. Phys. Solids 56, 1609–1623.